The Journal of Chemical Physics

Line shape parameters of PH_3 transitions: Theoretical studies of self-broadened widths and line mixing effects

Cite as: J. Chem. Phys. **152**, 214305 (2020); https://doi.org/10.1063/5.0008535
Submitted: 24 March 2020 . Accepted: 12 May 2020 . Published Online: 03 June 2020

C. Boulet, and Q. Ma

The Journal of Chemical Physics ARTICLE scitation.org/journal/jcp

Line shape parameters of PH_3 transitions: Theoretical studies of self-broadened widths and line mixing effects

Cite as: J. Chem. Phys. 152, 214305 (2020); doi: 10.1063/5.0008535
Submitted: 24 March 2020 • Accepted: 12 May 2020 •
Published Online: 3 June 2020

C. Boulet[1,a] and Q. Ma[2]

AFFILIATIONS

[1] Institut des Sciences Moléculaires d'Orsay (ISMO), CNRS, Université Paris-Saclay, Campus d'Orsay F-91405, France
[2] NASA/Goddard Institute for Space Studies and Department of Applied Physics and Applied Mathematics, Columbia University, 2880 Broadway, New York, New York 10025, USA

[a] **Author to whom correspondence should be addressed:** christian.boulet@u-psud.fr

ABSTRACT

Line mixing effects have been calculated in various parallel and perpendicular bands of self-broadened PH_3 lines and compared with recent experimental data. The theoretical approach is an extension to symmetric tops with high inversion barrier of the formalism previously developed for NH_3 [Q. Ma and C. Boulet, J. Chem. Phys. **144**, 224303 (2016)]. The model takes into account the non-diagonality of the scattering operator within the line space as well as, in a correct way, the double degeneracy of the j, k levels when $k \neq 0$. Transitions between such levels should be considered as doublets whose components may be coupled by the line mixing process. It has been shown that, at low pressure, the inversion of the experimental data will strongly depend on the splitting between the two components of a doublet. When it is significant, one can measure independently both the width of one component and the intra-doublet coupling matrix element. Otherwise, one can only measure the sum of these two elements. Comparisons with measurements show that the present formalism leads to accurate predictions of the experimental line shapes.

I. INTRODUCTION

PH_3 is a molecule of astrophysical interest since it has been observed in the atmospheres of Jupiter and Saturn[1,2] (mainly composed of H_2 and He). Accurate knowledge of the corresponding line shape parameters is important for remote sensing of these atmospheres, and PH_3 has been the subject of a large number of experimental investigations. In recent studies,[3,4] mainly devoted to the determination of positions and intensities of PH_3 transitions in the Pentad near 4 μm–5 μm, self-broadened widths, shifts, and line mixing parameters were also measured. Ten years earlier, similar measurements were made for the collisional broadenings in the ν_2 and ν_4 bands.[5] All these data give us the opportunity to apply the refined formalism developed for NH_3[6–9] to the calculation of these parameters for PH_3.

From the theoretical point of view, purely quantum approaches are impossible for such molecular systems. Therefore, most of the previous calculations of the pressure broadening parameters for such symmetric tops[5] have been performed in a semi-classical frame derived from the Anderson–Tsao–Curnutte (ATC)[10] formalism, including some improvements proposed by Robert and Bonamy (RB in the following),[11] as well as, more recently, "exact" trajectories and a more accurate description of the intermolecular potential[12] (an overview of similar studies can be found in Ref. 13). PH_3 has a pyramidal shape (point group C_{3v}) quite similar to that of NH_3, but its inversion barrier is considerably higher, leading, therefore, to a negligible inversion splitting. As a consequence, the rotational j, k levels with $k \neq 0$ are not necessarily split in two distinct sub-levels. As outlined by Cherkasov,[14,15] most of the previous studies devoted to pressure broadening of such symmetric tops have not correctly taken into account the consequences of that degeneracy.

We will show that a more correct treatment may be developed, thanks to some adjustments of our previous studies.[6–9] In

Sec. II, we outline some basic elements of the spectroscopy of PH_3. In Sec. III, we recall the principles of our formalism and their adjustments. Results are presented and discussed in Sec. IV. Section V summarizes the concluding remarks and perspectives.

II. BACKGROUND

A. Radiative selection rules

States are first defined by their symmetry species Γ in the C_{3v} group. Let us define by l_t the vibrational angular momentum associated with a given degenerate vibration t and by K, the component of the rotational angular momentum along the principal symmetry axis. The $K - \sum_t l_t = 3p$ levels (with $p = \pm1, \pm2, \ldots$) split into A_1 and A_2 components, while the levels with $K - \sum_t l_t \neq 3p$ give rise to a doubly degenerate wave functions pair of E symmetry.[16,17] As recalled in Ref. 16, the radiative transitions of symmetric tops with inversion symmetry obey the following rules (with $k = |K|$):
Parallel band: $\Delta k = 0$; $\Delta j = 0, \pm1$;
Perpendicular band: $\Delta k = \pm1$; $\Delta j = 0, \pm1$;
For the symmetry species: $A_1 \rightarrow A_2$, $A_2 \rightarrow A_1$, and $E_1 \rightarrow E_2$ or $E_2 \rightarrow E_1$.

B. Basis sets of the symmetric tops

In most of the studies of the energy levels of PH_3, Wang-type wave functions and a new definition of the symmetry species $A_\pm$ introduced in Ref. 17 allow an easier diagonalization of the internal Hamiltonian. The correspondence between these two symmetry definitions is recalled in the Appendix. As is well known, the wave functions of real symmetric tops also have to be eigenfunctions of the parity operator.[14,19] As an example, consider the ground vibrational level or any non-degenerate vibrational level. Parity adapted wave functions are defined by

$$|jkm\varepsilon\rangle = N_\varepsilon[|jkm\rangle + \varepsilon|j - km\rangle], \quad (1)$$

where k = 0, 1, 2, …, j. For k = 0, $N_\varepsilon = 1$; ε = 0. For k ≠ 0, $N_\varepsilon = 1/\sqrt{2}$. States are also defined by their symmetry species Γ (see the Appendix). When k is a multiple of three (k = 3p, with p = 1, 2, 3, …), Γ = A_+ or A_-. While for k ≠ 3p, Γ = E. Therefore, by using the definitions of Refs. 16–19, one may rewrite Eq. (1) as follows:

$$|jkmA_\pm\rangle = N_\varepsilon\Big[|jkm\rangle \pm (-1)^k|j - km\rangle\Big]. \quad (2)$$

For k = 3p, A-type splitting (also defined as A_1/A_2 splitting) of the two $A_\pm$ levels is observed mainly for k = 3 (but also in some cases for k = 6 and 9), which is caused by high order intra-molecular interactions. For the degenerate representation E, there is no splitting, and the degeneracy is not removed. The only important point is that one has to use basis wave functions having the symmetry of the C_{3v} group. Consequently, Eq. (2) can be generalized to the two $E_\pm$ states.

We now consider a degenerate vibrational level (for instance, $v_3^{\pm1}$, i.e., $v_3 = 1$ and $l_3 = \pm1$). By a similar approach (see the Appendix), for $k + l_3 = 3p$, the basis wave functions may be defined by

$$|v_3 l_3 jkmA_\pm\rangle = N_\varepsilon\Big[|v_3 l_3 jkm\rangle \pm (-1)^{k+l_3}|v_3 - l_3 j - km\rangle\Big], \quad (3)$$

and similar relations for the two degenerate E states ($k + l_3 \neq 3p$).

Of course, these wave functions are "zero order" ones since, contrarily to the calculation of accurate positions and intensities, it is not necessary for us to take into account the numerous intramolecular couplings that exist between the PH_3 states. As a consequence, we cannot perform calculations of the line shape parameters of "forbidden" Δk = 3p radiative transitions.

C. Preliminary qualitative analysis

Consider, in a parallel band, a **resolved** doublet where $k_i = k_f = 3$ and $j_f = j_i + 1$ [a QR(j_i, 3) doublet]. When the pressure increases, the two components of the doublet overlap leading, therefore, to a possible line mixing effect, if a significant W relaxation matrix element couples the two transitions.

Now, consider the case of an unresolved QR(j, k) line with k ≠ 3p. People calculating the intensity of such a line use the following procedure to take into account the k degeneracy: they calculate the intensity of the $E_1 \rightarrow E_2$ transition (for instance) and then multiply the result by two.[16] Such an approach, justified in the calculation of the intensity, is not at all valid when considering the collisional line shape. As shown by Cherkasov,[14,15] one has to think within the Liouville line space: if the two degenerate transitions $E_1 \rightarrow E_2$ and $E_2 \rightarrow E_1$ are collisionally coupled by using an off-diagonal element of the W matrix, the resulting line profile may be significantly altered by the line mixing of the two degenerate transitions.

III. THEORY

The formalism developed in Ref. 6 (noted as Paper I in the following) for parallel bands and in Ref. 9 (noted as Paper II) for perpendicular bands of NH_3 can be applied to the PH_3 molecule, just by changing the definition of the parity index ε, according to Eqs. (2) and (3).

A. Potential model

In the present work, the interaction between two PH_3 molecules [see Eq. (4) of Paper I[6]] has been represented by the sum of the dipole–dipole ($L_1 = L_2 = 1$; $K_1 = K_2 = 0$), dipole–quadrupole ($L_1 = 1$; $L_2 = 2$; $K_1 = K_2 = 0$), quadrupole–dipole ($L_1 = 2$; $L_2 = 1$; $K_1 = K_2 = 0$), and quadrupole–quadrupole ($L_1 = L_2 = 2$; $K_1 = K_2 = 0$) electrostatic components. All the corresponding parameters are given in Table I. We have used the parameters given in the study of Ref. 5, based on the RB formalism (i.e., ignoring the line coupling process). Note that we have neglected the weak vibrational dependence of the average vibrational value of all these parameters ($\langle v|X|v\rangle$). With respect to the isotropic part, driving the exact trajectory calculations, it is represented by a Lennard-Jones model whose parameters ε and σ have been determined from the viscosity data.[20]

TABLE I. Molecular parameters used in the calculations (from Ref. 5).

μ (D)	θ (DÅ)	ε (K)	σ (Å)	Molar mass (gr)
0.574	2.6	251.5	3.981	34

B. Ro-vibrational energy levels

The ro-vibrational energy levels and the transition wave numbers have been obtained from the HITRAN 2012 database[21] and from data bases kindly provided by I. Kleiner.[4]

C. Construction of the line subspaces

The size of the whole line space is determined by a cutoff defining the upper limits of the initial and final quantum numbers for the lines taken into account. In practice, in order to reduce an edge effect on the lines of interest, the cutoff has to be high enough. In the present study, we have included in the calculation all the lines contained in the HITRAN 2012 database. Meanwhile, based on our experiences in studying line mixing effects, we know that inter-branch coupling is much weaker than intra-branch coupling. Therefore, we have assumed that lines belonging to different branches are not coupled. In addition, all the components of the electrostatic potential obey the collisional selection rule $\Delta k = 0$, which coincides exactly with the radiative dipolar selection rule for parallel bands. Consequently, the whole line space can be divided into uncoupled subspaces, each corresponding to a given value of k and a given branch.

For perpendicular bands where the radiative and collisional selection rules differ, the construction of the sub-blocks is more complex and detailed in Paper II.[9]

D. A brief summary of the formalism

The matrix element of the relaxation operator can be expressed in terms of the average of the Liouville scattering operator over the internal degrees of the bath molecules, expressed via a second order cumulant expansion [see Eq. (3) of Paper I[6]],

$$W_{f'i'fi} = \frac{n_b \bar{v}}{2\pi c} \int_{r_{c,min}}^{\infty} dr_c 2\pi b \left(\frac{db}{dr_c}\right) \left[\delta_{f'f}\delta_{i'i} - \left\langle f'i' \left| e^{-S_2(r_c)} \right| fi \right\rangle\right]. \quad (4)$$

We neglect here the vibrational dependence of the isotropic potential so that S_1 is zero and does not appear in Eq. (4); n_b is the number density of the perturber, $\bar{v}$ is the average velocity, b is the impact parameter, and r_c is the distance of closest approach. Note that calculations have been restricted to the mean velocity without performing an average over the kinetic energy.

The general expressions of the various contributions to S_2, $S_{2,outer,i}$, $S_{2,outer,f}$, and $S_{2,middle}$ are given in Papers I[6] and II.[9] As is now well known, the non-diagonality of S_2 within the line space solely results from the $S_{2,middle}$ term. Its non-diagonal part, coupling transitions $i \to f$ and $i' \to f'$, is given by Eq. (11) of Paper I.[6] As detailed in Papers I[6] and II,[9] the magnitude of the off-diagonal elements of $S_{2,middle}$ depends on three factors:

- The first one is a coupling strength factor defined by [see Eq. (13) of Paper I[6]]

$$(-1)^{L_1}\sqrt{(2j_i+1)(2j'_i+1)(2j_f+1)(2j'_f+1)}\,W(j'_f j'_i j_f j_i, 1L_1) \times D^p(\varepsilon'_f j'_f k'_f \varepsilon_f j_f k_f; L_1 0) D^p(\varepsilon_i j_i k_i \varepsilon'_i j'_i k'_i; L_1 0), \quad (5)$$

  where the collisional transition matrix elements D^p are defined by Eq. (A3) of Paper I.[6]

- The two others are the arguments of the two dimensional (2D) potential correlation functions $F_{L_1 00 L_2 00}$ (defined in Appendix C of Paper I[6]): the frequency detuning between the two coupled lines, $\omega_{f'i'} - \omega_{fi}$, and the energy gap, $\frac{\omega_{i'i}+\omega_{f'f}}{2} + \omega_{i'_2 i_2}$, which takes into account the more or less resonant efficiency of the corresponding virtual transition. As shown in Paper I[6] (see Fig. 3), beyond its central region, the magnitude of $F_{L_1 00 L_2 00}$ decreases very quickly as its two arguments increase. In other words, the smaller these two gaps are, the stronger is the line coupling.

IV. RESULTS AND DISCUSSION

For parallel bands, calculation of the relaxation matrix W has been performed for the ν_2 band, while for perpendicular ones, we have considered the ν_3 band. In the NH_3 case, we have demonstrated a very important vibrational dependence of the W matrix.[8] It was a consequence of the very strong vibrational dependence of the inversion splitting, which may vary from about 0.8 cm^{-1} in the vibrational ground state up to 284 cm^{-1} in the $\nu_2 = 2$ state. As a consequence, the various arguments driving the amplitude of the various correlation functions (1-D: $\omega_{i'i} + \omega_{i'_2 i_2}$ or $\omega_{f'f} + \omega_{i'_2 i_2}$; 2-D: $\omega_{f'i'} - \omega_{fi}$ and $\frac{\omega_{i'i}+\omega_{f'f}}{2} + \omega_{i'_2 i_2}$) strongly vary when going from a given band to another one. This is not the case for the PH_3 bands under consideration: The A-splitting remains smaller than 0.1 cm^{-1} in any case and is zero for E–E transitions. Moreover, the vibrational dependence of the rotational constants is also too small to induce any significant vibrational effect. Therefore, the W matrix calculated for the ν_2 band is also valid for the other parallel bands, while that calculated for the ν_3 band can be used for the other perpendicular bands. Note that this explains why the widths observed in the ν_2 and ν_1 bands agree within 2%–4%, as shown in Table 5 of Ref. 4. However, as will be shown later on, if the W matrix elements are independent of vibration, calculation of the spectral profile will primarily depend on the frequency detuning.

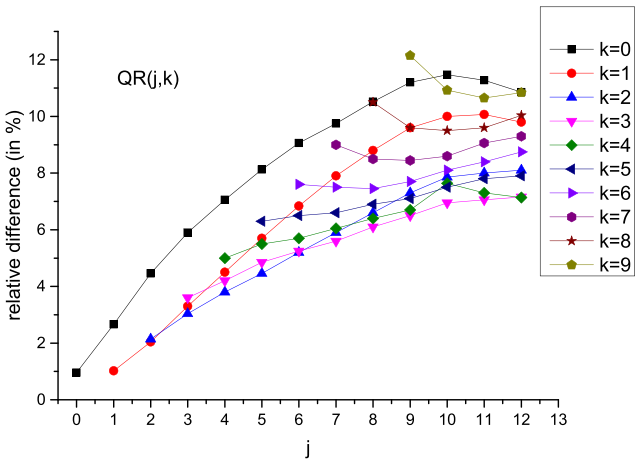

FIG. 1. Overestimation of calculated diagonal elements of W [i.e., 100 × ([$W_{no\ LC}$ − $W_{with\ LC}$]/$W_{with\ LC}$)] for QR(j, k) lines in the ν_2 band (LC means line coupling).

TABLE II. Some examples of the overestimation of the diagonal W_{ll} (in 10^{-3} cm^{-1} atm^{-1}) when compared to the experimental widths.

Transition	ν_1 band expt. Ref. 4	ν_2 band expt. Ref. 5	γ_l without LC	γ_l with LC
QR(2,1)	110	110.3	125.2	122.7
QR(7,5)	105.2	95.5	140	131.3
QR(8,7)	...	97.8	146.8	135.4
QR(9,4)	102.2	101.4	122.7	115
QR(9,9)	...	93.7	151.1	134.8
QR(10,7)	104.7	96.9	135.1	124.4
QR(12,9)	88.2	92.3	134	120.9
Transition	ν_3 band expt. Ref. 4	ν_4 band expt. Ref. 5	γ_l without LC	γ_l with LC
PP(7,4)	107.1	106.3	133.5	127.6
PP(8,5)	106	107.3	136	129

A. Overestimation of the W diagonal elements without line coupling

As will be shown later on, they do not necessarily correspond to the **observed** line widths, as opposed to the isolated line approximation, which neglects the non-diagonality of S_2 (no line coupling). This is, for instance, the case of the RB formalism. As it appears from Fig. 1 (where LC means line coupling), and in agreement with our previous studies, taking into account that non-diagonality slightly reduces the diagonal elements, $W_{ll} \equiv \gamma_l$ (where l is a shorthand notation for the set of quantum numbers of line l), which remains, however, significantly overestimated when compared to the experimental widths as it appears from Table II.

B. Calculated relaxation matrix

The off-diagonality of $S_{2,\text{middle}}$ reduces the diagonal elements and at the same time induces the off-diagonality of the W matrix. As expected, a given line is mainly coupled to its nearest neighbors as it appears from Table III and Fig. 2. As expected too, the intra-doublet elements have the largest amplitudes. This is a consequence of the very small frequency detuning between the two components of a doublet (when a significant A-splitting exists) and which falls to zero for E → E transitions, leading, in every case, to large magnitudes of the 2D correlation functions.

C. Calculation of the spectral line shape

This subsection is devoted to comparison between measured spectra and predictions of the present model and justifies the limitation of line mixing to intra-doublet coupling. As is well known, the purely collisional spectral profile, after eliminating Doppler as well as speed dependent effects and instrumental distortions, is given by[22]

$$F(\omega) = \frac{1}{\pi}\text{Im}\sum_{n,l} d_l \left\langle l \left| \frac{1}{\omega - L_0 - iW} \right| n \right\rangle d_n \rho_n. \tag{6}$$

For an optical transition n, d_n is the dipole reduced element, ρ_n is its relative population, and ω_n is its frequency. L_0 is diagonal and contains all these frequencies, and ω is the current frequency.

TABLE III. W matrix elements (in 10^{-3} cm^{-1} atm^{-1}) coupling a given line to its closest neighbors (recall that the collisional selection rule is $\Delta k = 0$, so that the k quantum number of the neighbor is not specified).

QQ(4, 3, A$_-$)	Neighbors QQ(j, symmetry)	3, A$_-$	3, A$_+$	4, A$_-$	4, A$_+$	5, A$_-$	5, A$_+$	6, A$_-$	6, A$_+$	7, A$_-$	7, A$_+$
	W matrix element	−7.68	−7.65	132.8	−28.5	−8.6	−9.8	−4.9	−6	−3.3	−3.3
QQ(7, 3, A$_+$)	Neighbors QQ(j, symmetry)	5, A$_-$	5, A$_+$	6, A$_-$	6, A$_+$	7, A$_-$	7, A$_+$	8, A$_-$	8, A$_+$	9, A$_-$	9, A$_+$
	W matrix element	−6.3	−5.2	−12.7	−9.1	−16.3	120.9	−9.	−13.7	−5	−6
QP(7, 6, A$_+$)	Neighbors QP(j, symmetry)	...	7, A$_-$	7, A$_+$	8, A$_-$	8, A$_+$	9, A$_-$	9, A$_+$	10, A$_-$	10, A$_+$	...
	W matrix element	...	−43.7	141.6	−7.3	−6.9	−3.4	−3.5	−1.7	−1.7	...
QP(8, 6, A$_+$)	Neighbors QP(j, symmetry)	...	7, A$_-$	7, A$_+$	8, A$_-$	8, A$_+$	9, A$_-$	9, A$_+$	10, A$_-$	10, A$_+$	...
	W matrix element	...	−7.3	−6.9	−35.4	137.5	−7.8	−7.4	−3.7	−3.8	...
QR(9, 9, A$_+$)	Neighbors QR(j, symmetry)	...	9, A$_-$	9, A$_+$	10, A$_-$	10, A$_+$	11, A$_-$	11, A$_+$	12, A$_-$	12, A$_+$	...
	W matrix element	...	−54.1	134.8	−10.6	−10.9	−4.3	−4.3	−1.6	−1.6	...

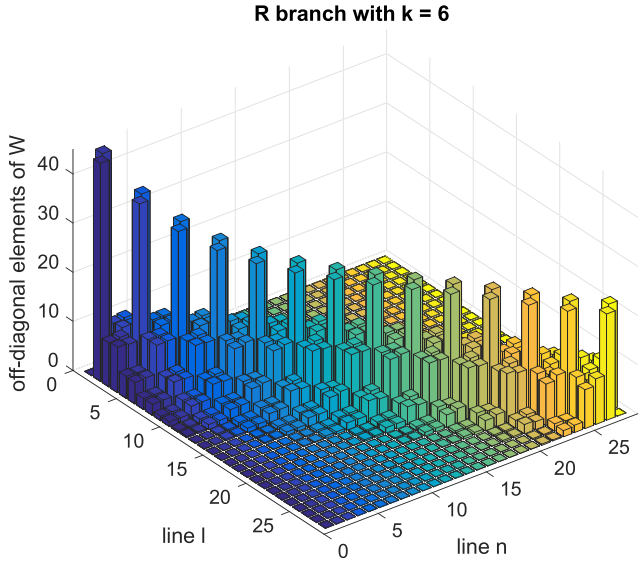

FIG. 2. Absolute values of the off-diagonal relaxation matrix elements $|W_{l,n}|$ (in 10^{-3} cm^{-1} atm^{-1}) for QR(j, k) lines in the k = 6 subspace. It contains 28 lines ordered as QR(6, 6, A_+), QR(6, 6, A_-), QR(7, 6, A_+), QR(7, 6, A_-), . . ., QR(19, 6, A_+), QR(19, 6, A_-). With this choice, the intra-doublet couplings are located at the super-diagonal elements (i.e., $W_{l,l+1}$ and $W_{l+1,l}$) (recall that *l* and *n* are short-hand notations for the set of quantum numbers of the lines).

As will be now demonstrated, the inversion of the $\omega - L_0 - iW$ matrix will mainly depend on both the intra-doublet frequency detuning and the pressure range of the experiments. In the measurements of Devi *et al.*,[4] the pressure varies between 2.048 Torr and 50.11 Torr, while it varies from 17 Torr to 50 Torr in the experiments of Salem *et al.*[5] Two situations must be distinguished:

(i) A significant A-splitting exists between the two components of the A–A doublet under consideration.
(ii) There is no splitting, which corresponds to the degenerate E–E doublets (and also when the A-splitting is negligible for A–A doublets).

Before considering these two cases, let us show that the inter-doublet couplings may be neglected in the ranges of pressure of the available experiments. As it appears from the two examples given in Table IV, a given doublet is always relatively well isolated from the other ones.

Therefore, if we forget, in a first step, the intra-doublet coupling, line mixing between the different doublets can be treated within the first order Rozenkranz approximation.[22] For a given line,

$$F_n(\omega) = \frac{1}{\pi}\frac{\gamma_n + Y_n(\omega-\omega_n)}{\gamma_n^2 + (\omega-\omega_n)^2}, \tag{7a}$$

$$Y_n = 2\sum{}'_{l\neq n}\frac{d_l}{d_n}\times\frac{W_{ln}}{\omega_n-\omega_l}. \tag{7b}$$

The prime in Eq. (7b) indicates that we exclude the intra-doublet contributions. The order of magnitude of the Y_n parameters can be estimated from our calculations. One obtains, for instance, $Y_n \approx -0.2\times10^{-2}$ atm^{-1} for QP(14, 3) and $Y_n \approx 0.8\times10^{-2}$ atm^{-1} for QQ(4, 3), since the QQ lines are more closely spaced. From Eq. (7a), the ratio of the dispersion to the Lorentzian component is given by $|Y_n(\omega-\omega_n)|/\gamma_n|$, which is equal for the worst above-mentioned case to about $0.07\times|\omega-\omega_n|$. In other words, the dispersive component will be of the order of 1% of the Lorentzian for detuning around 0.14 cm^{-1}, i.e., at least 17 times the line width, well outside the spectral range occupied by the line (recall that, at 50.11 Torr, $\gamma_n \cong 8\times10^{-3}$ cm^{-1}). Then, in the following, we will only consider the intra-doublet coupling.

1. First case: a significant A-splitting exists between the two components of a doublet.

In the following, the two components of the doublet are simply denoted by $|1\rangle$ and $|2\rangle$. Meanwhile, the diagonal elements of W are γ ($=\langle1|W|1\rangle = \langle2|W|2\rangle$), and the off-diagonal elements are ξ ($=\langle1|W|2\rangle = \langle2|W|1\rangle$). The frequency detuning is $\omega_2 - \omega_1 = 2\Delta\omega > 0$. A doublet belongs to that category of resolved doublet if $2\Delta\omega \geq \gamma$ in all the pressure ranges. As is known from the work of Ben Reuven,[23] the inversion of Eq. (6) in the 2 × 2 line space can be performed

TABLE V. Experimental and theoretical parameters for resolved doublets (in 10^{-3} cm^{-1} atm^{-1}).

Doublet	$\gamma_{expt.}$ Ref. 4	$\gamma_{calc.}$	$\xi_{expt.}$ Ref. 4	$\xi_{Calc.}$
ν_1 QP(14, 3)	100.4	79.3	−7.4	−9.6
$2\nu_4^0$ QQ(4, 3)	128.8	132.5	−25.8	−28.5
$2\nu_4^2$ PP(10, 9)	138.5	133	−46.9	−49.3
$2\nu_4^2$ PP(11, 9)	131.1	130	−39.5	−42
$2\nu_4^2$ PP(13, 9)	123.6	119	−29.1	−35.5
$2\nu_4^2$ PP(7, 6)	137.2	136.5	−36.2	−39.8
ν_3 RP(11, 3)	108.9	107.3	−7.1	−12.9
ν_3 PP(4, 3)	131.9	131.6	−26	−24.4
ν_3 PP(5, 3)	123.5	127.5	−16.9	−17.5
ν_3 PP(6, 3)	120.5	124.8	−12.2	−13.7

TABLE IV. Average distance between adjacent doublets (recall that, at 50.11 Torr, the width of each component is less than 10×10^{-3} cm^{-1}).

QQ(4, 3) ν_2 band	QQ(3, 3)	QQ(4, 3)	QQ(5, 3)	QQ(6, 3)	QQ(7, 3)
$(\omega_2 - \omega_1)$ cm^{-1}	+1.402	. . .	−1.7	−3.694	−5.935
QP(14, 3) ν_2 band	QP(12, 3)	QP(13, 3)	QP(14, 3)	QP(15, 3)	QP(16, 3)
$(\omega_2 - \omega_1)$ cm^{-1}	23.69	11.885	. . .	−11.934	−23.949

TABLE VI. Comparison of the observed widths with the present calculations (in 10^{-3} cm^{-1} atm^{-1}).

Transition	ν_1 band expt. Ref. 4	ν_2 band expt. Ref. 5	γ	ξ	$\gamma + \xi$
QR(2, 0)	110.5	112.1	112	...	112
QR(2, 1)	110	110.3	122.7	−8.3	114.4
QR(7, 0)	108.5	110.2	103.6	...	110.2
QR(7, 1)	105.7	105.8	107.1	−3.2	103.9
QR(7, 2)	107.3	103.8	113.7	−9.1	104.6
QR(7, 5)	105.2	95.5	131.3	−28.1	103.2
QR(8, 7)	...	97.8	135.4	−40.1	95.3
QR(9, 4)	102.2	101.4	115	−17.7	97.3
QR(9, 9)	...	93.7	134.8	−54.1	80.7
QR(10, 2)	100.9	100.4	95.4	−7.1	88.3
QR(10, 7)	104.7	96.9	124.4	−32	92.4
QR(12, 2)	96.5	94	79.1	−5.9	73.2
QR(12, 9)	88.2	92.3	120.9	−38.9	82
Transition	ν_3 band expt. Ref. 4	ν_4 band expt. Ref. 5	γ	ξ	$\gamma + \xi$
PP(7, 4)	107.1	106.3	127.6	−18.8	108.8
PP(8, 5)	106	107.3	129	−23.2	105.8

analytically. Assuming equal intensities for the two components and setting the origin of the current frequency ω at the mid-point of the spacing between the two components leads to

$$F(\omega) = \frac{2}{\pi} \frac{(\gamma+\xi)\omega^2 + (\gamma-\xi)(\Delta\omega^2 + \gamma^2 - \xi^2)}{(\omega^2 - \Delta\omega^2 + \xi^2 - \gamma^2)^2 + 4\gamma^2\omega^2}. \quad (8)$$

Of course, in the weak overlapping regime, Eq. (8) can be approximated by

$$F(\omega) = \frac{1}{\pi}\left[\frac{\gamma + Y_1(\omega-\omega_1)}{\gamma^2 + (\omega-\omega_1)^2} + \frac{\gamma + Y_2(\omega-\omega_2)}{\gamma^2 + (\omega-\omega_2)^2}\right], \quad (9a)$$

$$\text{with } Y_2 = -Y_1 = \frac{\xi}{\Delta\omega}. \quad (9b)$$

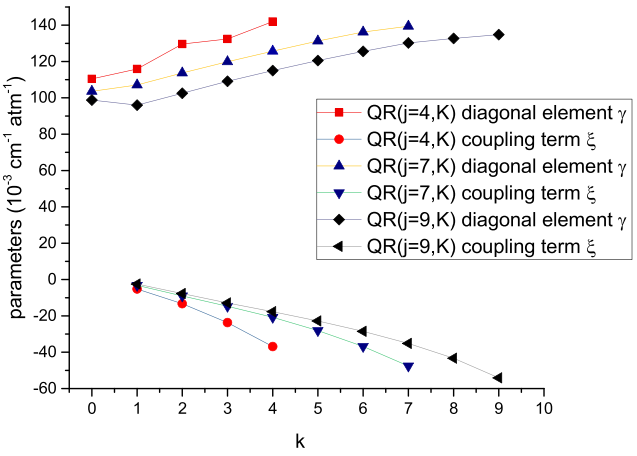

FIG. 3. Diagonal element γ and intra-doublet coupling ξ for some QR(j, k) doublets.

In other words, for such a doublet, it will be possible through a multi-spectrum fit to measure both γ **and** ξ independently. Table V gives the comparison of the measurements of Ref. 4 with our theoretical predictions. Most of the theoretical results agree acceptably well with the experimental data.

2. Second case: there is no splitting between the two components of a doublet.

When there is a significant coupling of the two components of a doublet ($\xi \neq 0$) but without splitting ($\Delta\omega = 0$), setting $\Delta\omega \to 0$ in

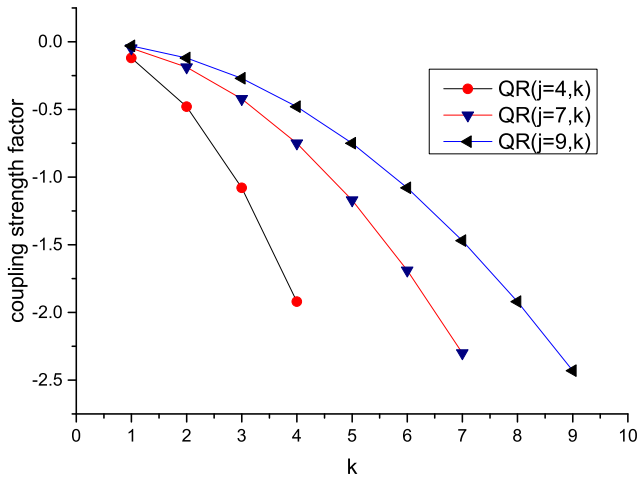

FIG. 4. The coupling strength factor [cf. Eq. (5)] associated with the intra-doublet coupling for some QR(j, k) doublets.

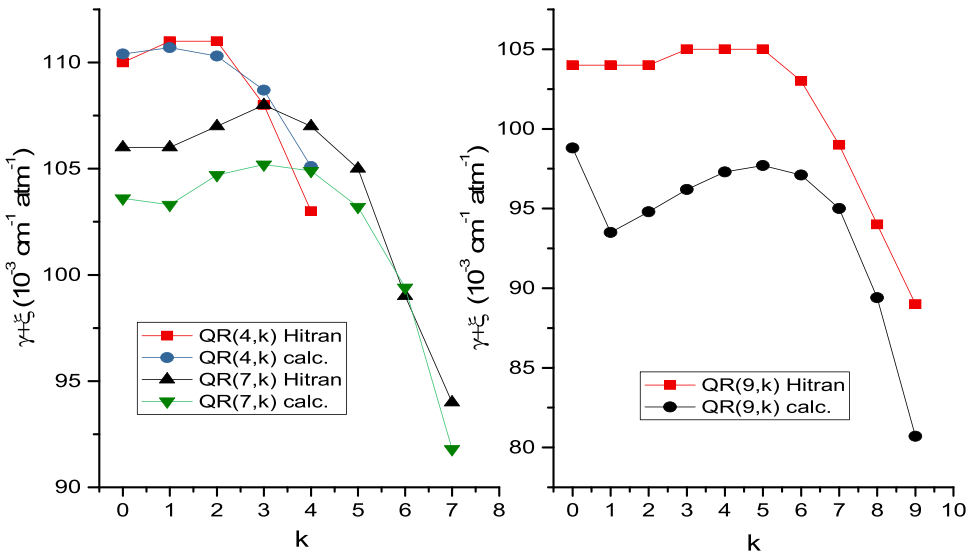

FIG. 5. Reduction in the line widths due to line mixing for degenerate doublets. Comparison of the HITRAN 2012 data with the theoretical predictions of γ + ξ.

Eq. (8) leads to the following profile for the degenerate line:

$$F(\omega) = \frac{2}{\pi}\frac{\gamma+\xi}{\omega^2+(\gamma+\xi)^2}. \quad (10)$$

Hence, due to line mixing, the two components of such a degenerate doublet merge into a single Lorentzian line whose half-width equals to $\gamma_{expt.} = \gamma + \xi$, the sum of the width of one of the component and of the coupling element. In other words, in that case, it is not possible to **independently** measure γ and ξ. The only parameter that can be obtained from any treatment of the experimental spectra is the sum of γ + ξ. Since ξ is negative, one begins to understand why the observed values as given in Table II were systematically smaller than γ. We present in Table VI a comparison between our calculated values of γ + ξ with the observed line widths.

As can be seen, the agreement between theory and experiment in now good with a few exceptions for the highest j values. This was not unexpected: when the rotational quantum numbers of the active molecule differ significantly from those of the most populated levels of the perturbers (here, $k_{2,max} = 0$; $j_{2,max} = 4$ at 296 K), most of the virtual transitions in the various S_2 components become less and less resonant. The magnitudes of the 1D and 2D correlation functions decrease quickly since their arguments increase. It is known that, under such conditions, it is not possible to limit the anisotropic potential to its longer range electrostatic part, which has to be completed by shorter range components.

The intra-doublet coupling reduces the observed widths by a very important amount, up to 40%, depending strongly on j, k values. Figures 3–5 give an illustration of the j, k dependences of γ, ξ, and γ + ξ, as well as a comparison with the experimental data from the HITRAN 2012 database.[21] For QR doublets, Fig. 3 gives γ and ξ as functions of k for three values of j. As may be seen, the amplitude of ξ reaches its maximum as j = k.

This can be easily understood by analyzing the amplitudes of the corresponding off-diagonal elements of $S_{2,middle}$. They are governed by the coupling strength factor [cf. Eq. (5)] plotted in Fig. 4. The strong resemblance between the j and k variation patterns of these coupling factors and the ξ matrix elements of Fig. 3 is clearly evidenced.

Figure 5 shows a comparison of the calculated values of γ + ξ with some observed widths. For j = 4 and 7, the theoretical values agree with the experimental ones within 2%. For j = 9, the agreement in not so good (10%). However, in any case, the general trends for the observed $\gamma_{expt}(j, k)$ are well predicted: for a given j value,

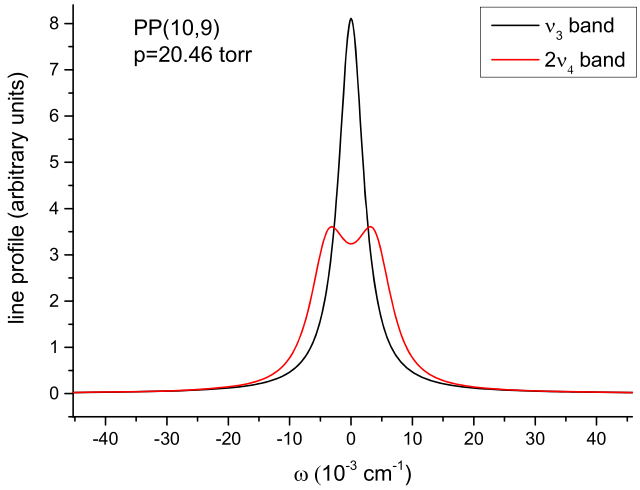

FIG. 6. Line profile of the PP(10, 9) doublet in the ν_3 and $2\nu_4^2$ bands. The frequency detuning between the two components of the doublet is 8.6×10^{-3} cm^{-1} in the $2\nu_4^2$ and zero in the ν_3 band.

TABLE VII. The PP(10, 9) doublet measured in different vibrational bands (in 10^{-3} cm^{-1} atm^{-1}). Experimental results from Ref. 4. The frequency detuning between the two components of the doublet is 8.6×10^{-3} cm^{-1} in the $2\nu_4^2$ band and allows the measurement of both the width of a component (γ_{expt}) and the coupling element (ξ_{expt}). In the ν_3 band, the detuning is zero and only $(\gamma + \xi)_{expt}$ can be measured.

$2\nu_4^2$	$\gamma_{expt} = 138.5$	$\xi_{expt} = -46.9$	$\gamma_{expt} + \xi_{expt} = 91.6$
ν_3	...	...	$(\gamma + \xi)_{expt} = 92$
Theory	$\gamma = 133$	$\xi = -49.3$	$\gamma + \xi = 83.7$

TABLE VIII. The QQ(4, 3) doublet measured in different vibrational bands. Experimental results for the $2\nu_4^0$ band come from Ref. 4 and from the HITRAN 2012 for the ν_1 and ν_2 bands. The frequency detuning between the two components of the doublet is 19.6×10^{-3} cm^{-1} in the $2\nu_4^0$ band and allows the measurement of both the width of a component (γ_{expt}) and the coupling element (ξ_{expt}). In the ν_1 and ν_2 bands, the detuning is zero and only $(\gamma + \xi)_{expt}$ can be measured.

$2\nu_4^0$	$\gamma_{expt} = 128.8$	$\xi_{expt} = -25.8$	$\gamma_{expt} + \xi_{expt} = 103$
ν_1 and ν_2	...	...	$(\gamma + \xi)_{expt} = 109$
Theory	$\gamma = 132.5$	$\xi = -28.5$	$\gamma + \xi = 104$

$\gamma_{expt}(j, k)$ increases slightly with k, to its maximum, then decreases to rather low values for k approaching j. Previous studies[24,25] were not able to explain that dependence and referred to various qualitative explanations. Here, the j, k dependence is just a consequence of the line mixing process between degenerate components. On that basis, it is easy to understand why there is no significant reduction in the widths when $k_i = 0$ because these lines do not have a doublet partner.

Finally, the PP(10, 9) and QQ(4, 3) doublets deserve a comment. PP(10, 9) has been measured in both the $2\nu_4^2$ and ν_3 bands.[4] As it appears from Fig. 6, measurements in the $2\nu_4^2$ band have allowed the determination of both γ and ξ (cf. Table V). Meanwhile, in the ν_3 band, the A-splitting is insignificant, so that only the sum $\gamma + \xi$ can be measured. As can be seen from Table VII, the measurements are fully consistent.

Similarly, for the QQ(4, 3) doublet, measurements in the $2\nu_4^0$ band where the doublet is resolved give γ and ξ, while for the ν_1 and ν_2 bands where the A-splitting is negligible, the HITRAN database gives only $\gamma + \xi$ (cf. Table VIII). Here also, the measurements (and the theory) are consistent, providing an additional test of the formalism.

V. CONCLUSION

In the present work, we have shown that the formalism of line mixing previously applied to NH_3 can be easily extended to symmetric tops with high inversion barrier. Following Green[19] and Cherkasov,[14] the k degeneracy of the rotational transitions has been taken into account through basis wave functions adapted to the full symmetry of the C_{3v} group. Then, the coupling of the two components of the resulting doublets has been shown to play a major role in the interpretation of the observed spectra. For E–E transitions and when the A splitting is not significant for A–A doublets, the line mixing process leads to an important decrease in the observed widths, when compared to a calculation based on the isolated line approximation. For A–A doublets with a significant splitting, it is possible to measure independently both the width of a component and the intra-doublet coupling element. In both situations, the theoretical model is in rather good agreement with all the available data.

Of course, the model also predicts inter-doublet coupling, but they do not influence the line shapes observed at low pressures. Testing the remaining part of the W relaxation matrix will require experiments at much higher pressures in order to reach a significant overlapping of the various doublets, as previously carried out for rare gas broadening of NH_3 bands.[26] Of course, the formalism can be easily extended to the more interesting case of foreign gas broadening since PH_3 has been mainly identified in the spectra of Jupiter and Saturn. The main challenge will be the introduction in the formalism of an intermolecular potential not limited to long-range components. For non-polar perturbers (H_2, N_2, rare gases, etc.), in the absence of *ab initio* sophisticated potentials, following Ref. 27, a solution could be the introduction of an atom–atom potential complementing the long-range part. From a theoretical point of view, it might be possible that the line mixing processes differ significantly from the self-broadening case analyzed here, due to different collisional propensity rules. However, the inversion of the experimental data, as a function of the intra-doublet detuning and the range of perturber pressure, as described in Sec. IV, will remain valid: when there is no splitting, one can only measure $\gamma + \xi$. When the splitting is significant, γ and ξ can be measured independently. Moreover, if the doublet can be analyzed within the first order Rozenkranz approximation [Eq. (9)], one should obtain $Y_2 = -Y_1 = \xi/\Delta\omega$. This is, for instance, what has been observed in Ref. 28 (Fig. 5) for the PH_3–H_2 system.

ACKNOWLEDGMENTS

The authors are grateful to Dr. I. Kleiner for her help in understanding the PH_3 spectroscopy and for providing some of her PH_3 databases. This research used resources of the National Energy Research Scientific Computing Center, which is supported by the Office of Science of the U.S. Department of Energy under Contract No. DE-AC02-05CH11231. Finally, the authors thank the referees for greatly improving the manuscript.

APPENDIX: SYMMETRY PROPERTIES OF THE WAVE FUNCTIONS

As recalled in Ref. 16, all the dipolar transitions must strictly obey the selection rules ($A_1 \rightarrow A_2$); ($A_2 \rightarrow A_1$); and ($E_1 \rightarrow E_2$) or ($E_2 \rightarrow E_1$), where A_1, A_2, and E correspond to the three irreducible representations of the C_{3v} group. In this appendix, we consider only wave functions of A_1 and A_2 symmetry.

As already mentioned [see Eqs. (2) and (3)], in most of the studies of the energy levels of PH_3, Wang-type wave functions are used, and a new definition of the symmetry species ($A_\pm$) are used.[17] Let us define by l_t the vibrational angular momentum associated with a given degenerate vibration t. The usual symmetry species A_{1or2} are related to the symmetries $A_\pm$ as follows:[16–18]

	$k + \sum_t l_t$ even		$k + \sum_t l_t$ odd	
	j even	j odd	j even	j odd
ψ_+	$A_1 = A_+$	$A_2 = A_+$	$A_2 = A_-$	$A_1 = A_-$
ψ_-	$A_2 = A_-$	$A_1 = A_-$	$A_1 = A_+$	$A_2 = A_+$

For a vibrational level with no excited angular momentum (i.e., the ground level), set $\sum_t l_t = 0$. For the vibrational level $v_3 = 1$; $l_3 = \pm 1$, set $\sum_t l_t = l_3$, etc.

DATA AVAILABILITY

The data that support the findings of this study are available from the corresponding author upon reasonable request.

REFERENCES

[1] V. Kunde, R. Hanel, W. Maguire, D. Gautier, J. P. Baluteau, A. Marten, A. Chedin, N. Husson, and N. Scott, Astrophys. J. **263**, 443 (1982).
[2] B. Bezard, P. Drossart, E. Lellouch, G. Tarrago, and J. P. Maillard, Astrophys. J. **346**, 509 (1989).
[3] V. Malathy Devi, I. Kleiner, R. L. Sams, L. R. Brown, D. C. Benner, and L. N. Fletcher, J. Mol. Spectrosc. **298**, 11 (2014).
[4] V. Malathy Devi, D. C. Benner, I. Kleiner, R. L. Sams, and L. N. Fletcher, J. Mol. Spectrosc. **302**, 17 (2014).
[5] J. Salem, H. Aroui, J.-P. Bouanich, J. Walrand, and G. Blanquet, J. Mol. Spectrosc. **225**, 174 (2004).
[6] Q. Ma and C. Boulet, J. Chem. Phys. **144**, 224303 (2016).
[7] C. Boulet and Q. Ma, J. Chem. Phys. **144**, 224304 (2016).
[8] Q. Ma, C. Boulet, and R. H. Tipping, J. Quant. Spectrosc. Radiat. Transfer **203**, 425 (2017).
[9] Q. Ma, C. Boulet, and R. H. Tipping, J. Chem. Phys. **146**, 134312 (2017).
[10] C. J. Tsao and B. Curnutte, J. Quant. Spectrosc. Radiat. Transfer **2**, 41 (1962).
[11] D. Robert and J. Bonamy, J. Phys. **40**, 923 (1979).
[12] C. Bray, D. Jacquemart, N. Lacome, M. Guinet, A. Cuisset, S. Eliet, F. Hindle, G. Mouret, F. Rohart, and J. Buldyreva, J. Quant. Spectrosc. Radiat. Transfer **116**, 87 (2013).
[13] J. Buldyreva, N. Lavrentieva, and V. Starikov, *Collisional Line Broadening and Shifting of Atmospheric Gases* (World Scientific Imperial College Press, London, 2010).
[14] M. R. Cherkasov, Opt. Spectrosc. **105**, 851 (2008).
[15] M. R. Cherkasov, Opt. Spectrosc. **106**, 1 (2009).
[16] G. Tarrago, O. N. Ulenikov, and G. Poussigue, J. Phys. **45**, 1429 (1984).
[17] G. Tarrago, Cah. Phys. **19**, 149 (1965).
[18] R. D. Schaeffer, R. W. Lovejoy, W. B. Olson, and G. Tarrago, J. Mol. Spectrosc. **128**, 135 (1988).
[19] S. Green, J. Chem. Phys. **73**, 2740 (1980).
[20] B. E. Poling, J. M. Prausnitz, and J. P. O'Connell, *Properties of Gases and Liquids*, 5th ed. (McGraw-Hill, NY, 2001).
[21] L. S. Rothman, I. E. Gordon, Y. Babikov *et al.*, J. Quant. Spectrosc. Radiat. Transfer **130**, 4 (2013).
[22] P. Rosenkranz, IEEE Trans. Antennas Propag. **23**, 498 (1975).
[23] A. Ben-Reuven, Phys. Rev. **145**, 7 (1966).
[24] C. Lerot, J. Walrand, G. Blanquet, J.-P. Bouanich, and M. Lepère, J. Mol. Spectrosc. **217**, 79 (2003).
[25] A. Levy, N. Lacome, and G. Tarrago, J. Mol. Spectrosc. **157**, 172 (1993).
[26] S. Hadded, F. Thibault, P.-M. Flaud, H. Aroui, and J. M. Hartmann, J. Chem. Phys. **120**, 217 (2004).
[27] J. Buldyreva, M. Guinet, S. Eliet, F. Hindle, G. Mouret, R. Bocquet, and A. Cuisset, Phys. Chem. Chem. Phys. **13**, 20326 (2011).
[28] J. Salem, G. Blanquet, M. Lepère, and R. b. Younes, Mol. Phys. **116**, 1280 (2018).